HiLo Microscopy with Caustic Illumination

GUORONG HU[1], JOSEPH GREENE[1], JIABEI ZHU[1], QIANWAN YANG[1], YUNZHE LI[1,†], JEFFREY ALIDO[1], RUIPENG GUO[1], AND LEI TIAN[1,2,*]

[1] Department of Electrical and Computer Engineering, Boston University, Boston, Massachusetts 02215, USA
[2] Department of Biomedical Engineering, Boston University, Boston, Massachusetts 02215, USA
[†] Current address: Department of Electrical Engineering & Computer Sciences, University of California, Berkeley, California 94720, USA
[*] leitian@bu.edu

Compiled June 8, 2023

HiLo microscopy is a widefield microscopy technique that provides optical sectioning by computationally combining two images, one with structured illumination and one with uniform illumination. The structured illumination can be achieved by various methods, such as speckle and periodic grids. In this work, we present a novel HiLo strategy that uses an off-the-shelf holographic diffuser and a low-coherence LED source to create random caustic patterns. This method has several advantages over existing ones, such as simplicity and cost-effectiveness. We achieve 4.5 µm optical sectioning capability and demonstrate the performance of our method by imaging a thick and highly scattering brain section. We anticipate that our caustic-based structured illumination approach will enhance the versatility of HiLo microscopy and extend to various imaging applications.

http://dx.doi.org/10.1364/ao.XX.XXXXXX

Widefield fluorescence microscopy is indispensable for studying biological structures and dynamics. However, this technique is inherently susceptible to out-of-focus fluorescence background due to the "missing cone" in the 3D optical transfer function (OTF) [1]. Optical sectioning (OS) techniques have been developed to address this issue, enabling the removal of fluorescence background and enhancing image contrast, while also facilitating high-fidelity 3D imaging [2]. Various approaches have been proposed to achieve OS, such as confocal microscopy [3], light sheet microscopy [4]), and structured illumination microscopy (SIM) [5]. Our focus lies on OS SIM techniques that can be implemented with relatively simple setups. For example, the first OS SIM technique utilized a 1D grid pattern, reconstructing each optically sectioned image by combining images acquired with three 120° phase-shifted patterns [5]. HiLo, another OS SIM method, simplifies the imaging requirements by capturing two images – one with a uniform pattern and the other with a structured pattern [6]. However, existing illumination strategies in HiLo rely on either laser source [6, 7] or intensity modulation with a digital micro-mirror device (DMD) [8]. Here, we present a caustic illumination-based approach that effectively reduces the hardware requirements of the HiLo technique by employing an off-the-shelf holographic diffuser and an LED source.

Our experimental setup is shown in Figure 1. It includes a collimated LED (central wavelength λ = 470 nm, Thorlabs M470L5) as the light source, a backside-illuminated CMOS sensor (4000 × 3000 pixels, pixel size: 1.85 µm, The Imaging Source DFM 37UX226-ML) for image capture, and a fluorescence filter set (Thorlabs MF469-35, MF525-39, and MD498) to separate excitation and emission. Uniform illumination in the excitation path is formed in the same manner as in standard epi-fluorescence microscopy, while structured illumination is generated by inserting a holographic diffuser (Edmund Optics 47-988) after the light source. The resulting caustic patterns are projected onto the sample plane using a relay system (f_1 = 300 mm, f_2 = 180 mm, Thorlabs ACT508-300-A, AC508-180-A) and a microscope (objective: 20× 0.75 NA, Nikon TE2000-U). Axial scanning is automated by rotating the microscope's fine focus knob with a step motor (Thorlabs MFC 1). The collected fluorescence passes through the same microscope and another relay system (f_2 = f_3 = 180 mm, Thorlabs ACT508-180-A) before reaching the sensor.

To compute the optically sectioned image, we adapted two existing HiLo algorithms [7, 9], which process the uniformly illuminated image $I_u(\vec{\rho})$ and the caustic-illuminated image $I_s(\vec{\rho})$. The resulting optically sectioned HiLo image $I_{\mathrm{HiLo}}(\vec{\rho})$ combines the in-focus high-frequency components $I_{\mathrm{Hi}}(\vec{\rho})$ and in-focus low-frequency components $I_{\mathrm{Lo}}(\vec{\rho})$, where $\vec{\rho}$ denotes the 2D spatial coordinate. $I_{\mathrm{Hi}}(\vec{\rho})$ is directly extracted from $I_u(\vec{\rho})$ using a high-pass Gaussian filter $HP[\cdot]$ since the high-frequency components in $I_u(\vec{\rho})$ are inherently in focus:

$$I_{\mathrm{Hi}}(\vec{\rho}) = HP[I_u(\vec{\rho})], \tag{1}$$

where the cut-off frequency of the filter $\vec{k_h}$ is defined by $HP(\vec{k_h}) = 1/2$. On the other hand, $I_{\mathrm{Lo}}(\vec{\rho})$ is extracted through several steps since simple low-pass filtering to $I_u(\vec{\rho})$ does not reject out-of-focus background. First, the normalized raw images are subtracted to remove variations from the object itself, retaining information proportional to the caustic illumination:

$$I_d(\vec{\rho}) = \frac{I_s(\vec{\rho})}{LP_d[I_s(\vec{\rho})]} - \frac{I_u(\vec{\rho})}{LP_d[I_u(\vec{\rho})]}, \tag{2}$$

where $LP_d[\cdot]$ is a low-pass Gaussian filter with a cut-off frequency $\vec{k_l}$ defined similarly to $\vec{k_h}$. As the caustic contrast decays as a function of defocus, the absolute value of $I_d(\vec{\rho})$ is able to

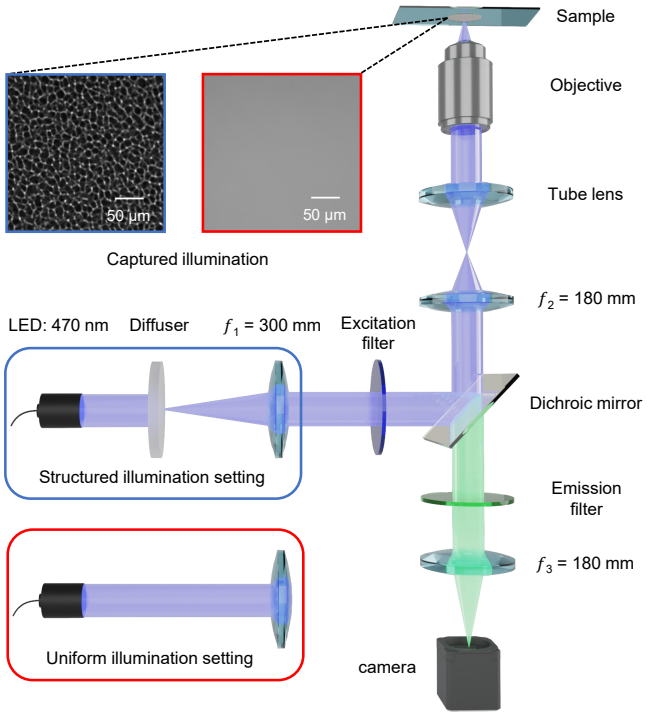

Fig. 1. Setup of caustic-illumination HiLo microscopy. The caustic pattern is generated by inserting a holographic diffuser into the excitation path. Insets: example uniform and caustic illumination patterns imaged with a uniform fluorescent layer.

resolve axial information. Additionally, the OS capability can be further tuned by applying an extra bandpass filter to $I_d(\vec{\rho})$:

$$W(\vec{k_\perp}) = \exp\left(-\frac{|\vec{k_\perp}|^2}{2\sigma_w^2}\right) - \exp\left(-\frac{|\vec{k_\perp}|^2}{\sigma_w^2}\right), \tag{3}$$

where $\vec{k_\perp}$ is the 2D frequency coordinate. Finally, the contrast map extracted from $I_d(\vec{\rho})$ is

$$C_n(\vec{\rho}) = \left|\mathcal{F}^{-1}\left\{W(\vec{k_\perp}) \times \mathcal{F}\left\{I_d(\vec{\rho})\right\}\right\}\right|, \tag{4}$$

where $\mathcal{F}\{\cdot\}$ and $\mathcal{F}^{-1}\{\cdot\}$ denote the Fourier and inverse Fourier transforms, respectively. However, $C_n(\vec{\rho})$ includes the effects of noise, as shot noise and readout noise introduce additional variations in $I_u(\vec{\rho})$ and $I_s(\vec{\rho})$, resulting in a bias when quantifying the contrast. To account for this, the camera gain G (unit: e-/ADU) and readout noise level σ_r (unit: e-) are calibrated, and the bias is calculated as

$$\begin{aligned}
\sigma_{I_u}^2(\vec{\rho}) &= \left(\frac{1}{LP_d[I_u(\vec{\rho})]}\right)^2 \left[\frac{I_u(\vec{\rho})}{G} + \left(\frac{\sigma_r}{G}\right)^2\right], \\
\sigma_{I_s}^2(\vec{\rho}) &= \left(\frac{1}{LP_d[I_s(\vec{\rho})]}\right)^2 \left[\frac{I_s(\vec{\rho})}{G} + \left(\frac{\sigma_r}{G}\right)^2\right], \\
\sigma_n^2(\vec{\rho}) &= \frac{1}{4\pi^2}\left(\sigma_{I_u}^2(\vec{\rho}) + \sigma_{I_s}^2(\vec{\rho})\right) \int |W(\vec{k_\perp})|^2 d^2\vec{k_\perp}.
\end{aligned} \tag{5}$$

The corrected contrast map is then obtained as

$$C(\vec{\rho}) = \sqrt{C_n^2(\vec{\rho}) - \sigma_n^2(\vec{\rho})}. \tag{6}$$

This local contrast is higher for in-focus components compared to out-of-focus components. By first multiplying $C(\vec{\rho})$ with $I_u(\vec{\rho})$, and then low-pass filtering using $LP[\cdot]$, the in-focus low-frequency components are obtained:

$$I_{\mathrm{Lo}}(\vec{\rho}) = LP[C(\vec{\rho}) \times I_u(\vec{\rho})], \tag{7}$$

where $LP[\cdot] = 1 - HP[\cdot]$ is the complementary low-pass filter. The HiLo image is synthesized by fusing $I_{\mathrm{Lo}}(\vec{\rho})$ and $I_{\mathrm{Hi}}(\vec{\rho})$:

$$I_{\mathrm{HiLo}}(\vec{\rho}) = \eta I_{\mathrm{Lo}}(\vec{\rho}) + I_{\mathrm{Hi}}(\vec{\rho}), \tag{8}$$

where $\eta = \mathcal{F}\left\{I_{\mathrm{Hi}}(\vec{\rho})\right\}(\vec{k_h}) / \mathcal{F}\left\{I_{\mathrm{Lo}}(\vec{\rho})\right\}(\vec{k_h})$, set as the ratio between the pair of spectra at the cutoff frequency $\vec{k_h}$, allowing for a smooth transition in the Fourier domain. The algorithm includes three tunable parameters: $\vec{k_l}$, σ_w, and $\vec{k_h}$.

To quantitatively estimate the OS capability and determine the optimal parameters in our caustic-HiLo system, we captured a z stack of caustic patterns using a thin fluorescent sample (Rhodamine 123 dissolved in water, Thermo Fisher Scientific). The sample was scanned axially over a range of 90 µm with a step size of 0.1 µm. Figure 2a shows the 2D Fourier transform of an in-focus caustic pattern, where the white dashed line represents the system bandwidth. Throughout this paper, all frequencies are normalized by $1/k_0$, where $k_0 = 2\pi/\lambda$, unless stated otherwise. We computed the radial average of the frequency components, as shown in Figure 2b. By defining the threshold of the bandwidth as a 3 dB amplitude attenuation from the maximum, we determined that the pattern primarily occupies low frequencies with a peak at 0.048 and a bandwidth of 0.028 (lower bound: 0.032; upper bound: 0.06). As the goal of $LP_d[\cdot]$ is to remove the caustic pattern while preserving the object information, we set $\vec{k_l}$ to be the lower bound of the pattern's bandwidth.

To characterize the OS capability using the measured caustic pattern stack, we calculated the pattern contrast as a function of the defocus distance. We applied an optional bandpass filter layer-wise to fine-tune the sectioning curve. According to Eq. (3), $W(\vec{k_\perp})$ reaches its maximum at the frequency $|\vec{k_\perp}| = \sqrt{2\ln 2}\sigma_w$. Therefore, we selected six equally spaced values of σ_w between 0.012 and 0.162 with a step of 0.03 to cover the entire range of spatial frequencies in the caustic pattern. Among these values, when $\sigma_w = 0.042$, the maximum of $W(\vec{k_\perp})$ coincides with the primary frequency of the caustic pattern, indicating minimal effect on the original pattern. Figure 2c illustrates three representative filters ($\sigma_w = 0.012, 0.042, 0.162$) along with the simulated in-focus 2D OTF of the system. Figure 2d displays the corresponding sectioning curves with σ_w values shown in Figure 2c, as well as without σ_w. Two observations can be made. First, all curves exhibit a secondary peak near the focus due to the holographic diffuser's two sets of axially displaced foci that are approximately symmetric about the diffuser plane. In our experiment, the separation between the two focal planes was measured to be 12.7 mm. Second, $W(\vec{k_\perp})$ not only reshapes the sectioning curves but also shifts them, especially for small σ_w. This occurs because out-of-focus images contain more low-frequency components compared to an in-focus image. With a small σ_w, $W(\vec{k_\perp})$ suppresses the majority of frequencies in the in-focus image while retaining most of them in the out-of-focus images.

We further measured the-full-width-at-half maximum (FWHM) of all the sectioning curves and plotted them in Figure 2e. The solid blue line represents the FWHM without σ_w (FWHM = 7.5 µm). As σ_w increases, the FWHM decreases,

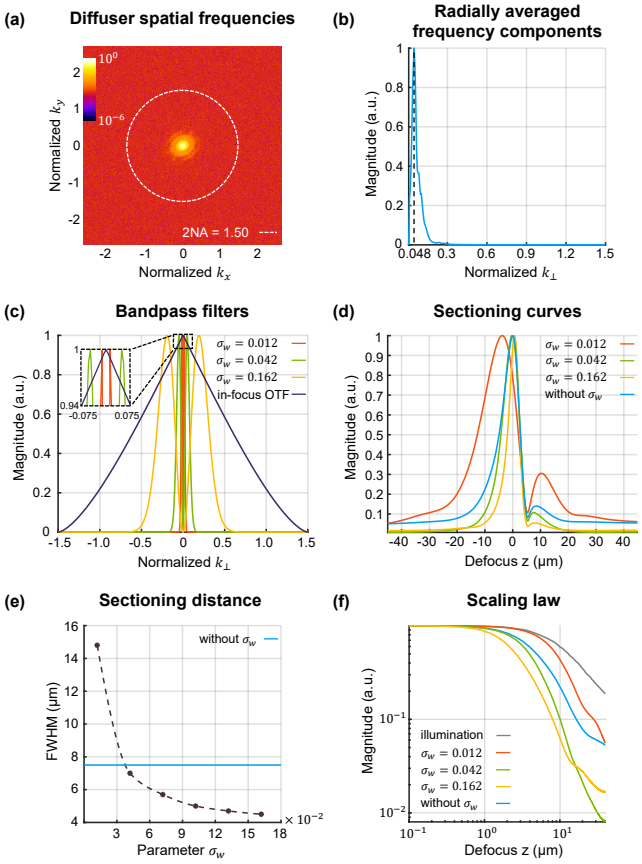

Fig. 2. Sectioning capability analysis. (a) 2D Fourier transform of the in-focus caustic pattern. (b) The radial average of (a) shows the diffuser's bandwidth and primary frequency. (c) Comparison between the in-focus OTF and bandpass filters having different σ_w values. (d) Contrast decay calculated from a z stack of caustic patterns with each layer prefiltered to tune the sectioning range. (e) The FWHM of the sectioning curves as a function of σ_w. The sectioning range without filtering is 7.5 μm. (f) Contrast decay on a log-log scale within the range of 0 to -40 μm.

asymptotically approaching 4.5 μm ($\sigma_w = 0.162$). This behavior differs from speckle-HiLo microscopy, where σ_w linearly affects the sectioning, since a speckle pattern has a flat spectrum within the system bandwidth [9].

The sectioning quantified in Figure 2e is only applied to $I_{\mathrm{Lo}}(\vec{\rho})$ through Eq. (7). To ensure the same sectioning range is obtained for $I_{\mathrm{Hi}}(\vec{\rho})$, we selected $\vec{k_h}$ so that the axial bandwidth of OTF$(\vec{k_h}, k_z)$ matches the desired sectioning range. Based on the Stokseth approximation [10], we found that $\vec{k_h} \approx 0.06$ without σ_w and $\vec{k_h} \approx 0.1$ when $\sigma_w = 0.162$.

Next, we estimated the scaling law of the OS for our caustic-HiLo technique. To do this, the sectioning curves illustrated in Figure 2d were rearranged. We aligned the maxima of all the curves and confined the range from 0 to -40 μm to mitigate the influence of the twin foci. In order to study the sectioning effect from the structured illumination alone, we captured another caustic stack by positioning a camera directly at the front focal plane of the tube lens and moving the diffuser in a 1-mm step over a 100-mm range. This stack was then converted to the sample plane and interpolated to the same z step as the

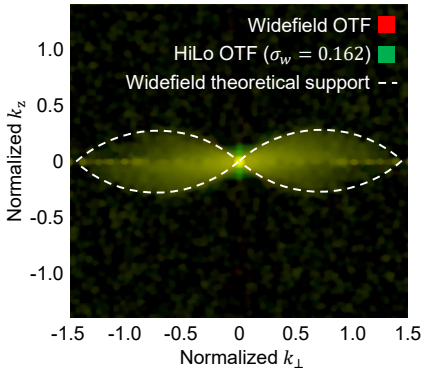

Fig. 3. The experimentally measured HiLo 3D OTF expands the support around the zero frequency (sample: 200 nm bead).

fluorescent caustic stack. All the contrast decay curves were displayed on a log-log scale in Figure 2f, following the method in [11]. Due to the properties of the diffuser, the scaling lines are not strictly linear, and different σ_w values change the slope as well. Despite this, we made basic estimates. As depicted by the gray curve, which represents the sectioning due to the illumination alone, the pattern contrast scales approximately as $z^{-0.8}$ for large defocus distance z. After the acceleration of the detection OTF, the contrast decay follows approximately a $z^{-1.5}$ relationship shown by the blue curve. With the additional $W(\vec{k_\perp})$ ($\sigma_w = 0.162$), the yellow line decays around z^{-2}. This is in contrast to speckle-HiLo technique in which the illumination contrast remains constant, and thus the sectioning is entirely provided by the detection OTF, which follows a z^{-1} relationship without the bandpass filter and a $z^{-1.5}$ relationship with the bandpass filter [9].

Next, we performed the point spread function (PSF) calibration using a 200-nm fluorescent bead (Phosphorex) over a range of 90 μm with a step size of 0.1 μm. The experimental widefield 3D OTF was obtained directly by applying a 3D Fourier transform to the widefield PSF stack. To compute the HiLo 3D OTF, we applied a slightly modified HiLo process to the widefield PSF stack as follows: 1. high-pass filtering the widefield PSF to obtain $\mathrm{PSF}_{\mathrm{Hi}}(\vec{\rho}, z)$; 2. multiplying the widefield PSF with the sectioning curve ($\sigma_w = 0.162$), followed by low-pass filtering, resulting in $\mathrm{PSF}_{\mathrm{Lo}}(\vec{\rho}, z)$; 3. combining $\mathrm{PSF}_{\mathrm{Hi}}(\vec{\rho}, z)$ and $\mathrm{PSF}_{\mathrm{Lo}}(\vec{\rho}, z)$ to generate $\mathrm{PSF}_{\mathrm{HiLo}}(\vec{\rho}, z)$; 4. finally, applying a 3D Fourier transform to obtain the HiLo 3D OTF. In Figure. 3, we present the overlay of the two OTFs. The widefield OTF shows a good agreement with the theory. The HiLo OTF predominantly overlaps with the widefield OTF, with the exception of expanded frequency support around the zero frequency, effectively filling the missing cone and thereby providing OS.

Finally, we applied our technique to image a mouse brain cortex tissue section (approximately 400 μm thick), where a specific subset of inhibitory interneurons expressed GCaMP6f (Figure. 4). We acquired two co-localized image stacks using uniform and caustic illumination, respectively, with a range of 100 μm and a step size of 0.5 μm. The field of view (FOV) measured 370 × 278 μm. During image acquisition, we utilized an illumination power of 7.5 mW at the sample plane and set the exposure time to 1 second. The resulting paired images were processed to generate two HiLo stacks: one without applying

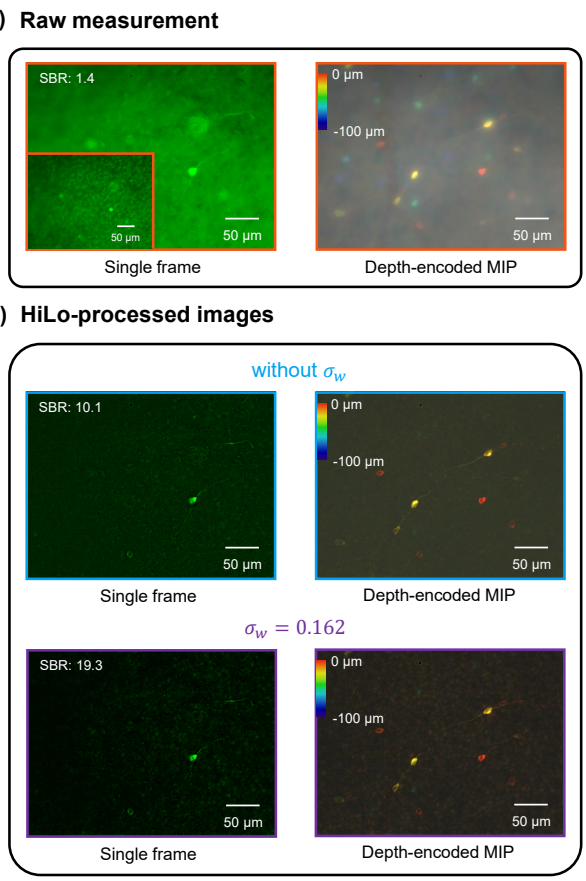

Fig. 4. Experimental results on a mouse brain cortex slice. Two image stack pairs with uniform and caustic illumination were acquired. (a) Example raw measurement. Inset: example image with structured illumination. (b) After HiLo processing without σ_w and with $\sigma_w = 0.162$, the example co-localized frames improve SBR by 7× and 13×, respectively. In (a) and (b), the depth-encoded MIPs from the widefield and the HiLo stacks are presented for comparison.

σ_w and the other with $\sigma_w = 0.162$. As a final denoising step, we employed a median filter. Some residual illumination patterns remained in the final results. To evaluate the OS improvement, we calculated the signal-to-background ratio (SBR) for both the widefield image and the co-localized HiLo images. The SBR represents the ratio of the average neuronal signal to the average background fluorescence within a defined region of interest (ROI). For the widefield image, the SBR was 1.4. After applying the HiLo technique, the SBR improved by 7× without using a bandpass filter, and by 13× with a bandpass filter having $\sigma_w = 0.162$. Additionally, we also compared the depth-encoded maximum intensity projection (MIP) among the widefield stack and the two HiLo stacks, in which hue represents depths and saturation represents intensity. Due to the presence of strong scattering, the contrast of patterns diminished when imaging at deeper layers. Consequently, although neurons in deeper layers were visible in the widefield stack, the algorithm still treated them as out-of-focus signals and removed them.

In conclusion, we have introduced a novel illumination approach for HiLo microscopy. The proof-of-concept demonstration achieved OS of 4.5 µm. We experimentally validated the technique on a thick, highly scattering brain tissue section. By utilizing an off-the-shelf diffuser and an LED source, our structured illumination module offers a straightforward, compact, and cost-effective solution that holds promise for diverse imaging applications.

Funding. National Institutes of Health (R01NS126596).

Acknowledgments. The authors thank Shuqi Zheng and Sheng Xiao for helpful discussion on HiLo microscopy, as well as Kevin J. Monk, Brett T. DiBenedictis, Ian G. Davison for providing the brain tissue section.

Disclosures. The authors declare no conflicts of interest.

REFERENCES

1. J. Mertz, *Introduction to optical microscopy* (Cambridge University Press, 2019).
2. J. Mertz, Optica **6**, 1261 (2019).
3. J. Pawley, *Handbook of biological confocal microscopy*, vol. 236 (Springer Science & Business Media, 2006).
4. B.-C. Chen, W. R. Legant, K. Wang, L. Shao, D. E. Milkie, M. W. Davidson, C. Janetopoulos, X. S. Wu, J. A. Hammer III, Z. Liu *et al.*, Science **346**, 1257998 (2014).
5. M. A. Neil, R. Juškaitis, and T. Wilson, Opt. letters **22**, 1905 (1997).
6. D. Lim, K. K. Chu, and J. Mertz, Opt. letters **33**, 1819 (2008).
7. T. N. Ford, D. Lim, and J. Mertz, J. biomedical optics **17**, 021105 (2012).
8. R. Shi and L. Kong, J. Phys. D: Appl. Phys. **54**, 414001 (2021).
9. D. Lim, T. N. Ford, K. K. Chu, and J. Mertz, J. biomedical optics **16**, 016014 (2011).
10. P. A. Stokseth, JOSA **59**, 1314 (1969).
11. C. Ventalon, R. Heintzmann, and J. Mertz, Opt. letters **32**, 1417 (2007).

FULL REFERENCES

1. J. Mertz, *Introduction to optical microscopy* (Cambridge University Press, 2019).
2. J. Mertz, "Strategies for volumetric imaging with a fluorescence microscope," Optica **6**, 1261–1268 (2019).
3. J. Pawley, *Handbook of biological confocal microscopy*, vol. 236 (Springer Science & Business Media, 2006).
4. B.-C. Chen, W. R. Legant, K. Wang, L. Shao, D. E. Milkie, M. W. Davidson, C. Janetopoulos, X. S. Wu, J. A. Hammer III, Z. Liu *et al.*, "Lattice light-sheet microscopy: imaging molecules to embryos at high spatiotemporal resolution," Science **346**, 1257998 (2014).
5. M. A. Neil, R. Juškaitis, and T. Wilson, "Method of obtaining optical sectioning by using structured light in a conventional microscope," Opt. letters **22**, 1905–1907 (1997).
6. D. Lim, K. K. Chu, and J. Mertz, "Wide-field fluorescence sectioning with hybrid speckle and uniform-illumination microscopy," Opt. letters **33**, 1819–1821 (2008).
7. T. N. Ford, D. Lim, and J. Mertz, "Fast optically sectioned fluorescence hilo endomicroscopy," J. biomedical optics **17**, 021105–021105 (2012).
8. R. Shi and L. Kong, "Evaluating structured-illumination patterns in optimizing optical-sectioning of hilo microscopy," J. Phys. D: Appl. Phys. **54**, 414001 (2021).
9. D. Lim, T. N. Ford, K. K. Chu, and J. Mertz, "Optically sectioned in vivo imaging with speckle illumination hilo microscopy," J. biomedical optics **16**, 016014–016014 (2011).
10. P. A. Stokseth, "Properties of a defocused optical system," JOSA **59**, 1314–1321 (1969).
11. C. Ventalon, R. Heintzmann, and J. Mertz, "Dynamic speckle illumination microscopy with wavelet prefiltering," Opt. letters **32**, 1417–1419 (2007).